Naphthodithiophene-Based Nonfullerene Acceptor for High-Performance Organic Photovoltaics: Effect of Extended Conjugation

Jingshuai Zhu, Zhifan Ke, Qianqian Zhang, Jiayu Wang, Shuixing Dai, Yang Wu, Ye Xu, Yuze Lin, Wei Ma, Wei You, and Xiaowei Zhan**

Naphtho[1,2-*b*:5,6-*b*′]dithiophene is extended to a fused octacyclic building block, which is end capped by strong electron-withdrawing 2-(5,6-difluoro-3-oxo-2,3-dihydro-1H-inden-1-ylidene)malononitrile to yield a fused-ring electron acceptor (IOIC2) for organic solar cells (OSCs). Relative to naphthalene-based IHIC2, naphthodithiophene-based IOIC2 with a larger π-conjugation and a stronger electron-donating core shows a higher lowest unoccupied molecular orbital energy level (IOIC2: −3.78 eV vs IHIC2: −3.86 eV), broader absorption with a smaller optical bandgap (IOIC2: 1.55 eV vs IHIC2: 1.66 eV), and a higher electron mobility (IOIC2: 1.0×10^{-3} cm^2 V^{-1} s^{-1} vs IHIC2: 5.0×10^{-4} cm^2 V^{-1} s^{-1}). Thus, IOIC2-based OSCs show higher values in open-circuit voltage, short-circuit current density, fill factor, and thereby much higher power conversion efficiency (PCE) values than those of the IHIC2-based counterpart. In particular, as-cast OSCs based on FTAZ: IOIC2 yield PCEs of up to 11.2%, higher than that of the control devices based on FTAZ: IHIC2 (7.45%). Furthermore, by using 0.2% 1,8-diiodooctane as the processing additive, a PCE of 12.3% is achieved from the FTAZ:IOIC2-based devices, higher than that of the FTAZ:IHIC2-based devices (7.31%). These results indicate that incorporating extended conjugation into the electron-donating fused-ring units in nonfullerene acceptors is a promising strategy for designing high-performance electron acceptors.

Solution-processed organic solar cells (OSCs) have attracted considerable attention from industry and academia because of their advantages such as light weight, low cost, flexibility, and transparency.[1–6] Fullerene derivatives, such as phenyl-C_{61}-butyric acid methyl ester ($PC_{61}BM$) and phenyl-C_{71}-butyric acid methyl ester ($PC_{71}BM$), are widely used electron acceptors in bulk heterojunction (BHJ) OSCs due to their isotropic charge transport and high electron mobility during the past two decades.[7–9] Nevertheless, fullerene derivatives suffer from some insufficiencies such as limited energy level tunability, weak absorption in the visible region, and morphology instability, which restrict the further development of BHJ OSCs.[10,11]

In 2015, we reported the original fused-ring electron acceptors (FREAs) with acceptor–donor–acceptor (A–D–A) structure based on indacenodithiophene or indacenodithienothiophene end-capped with 1,1-dicyanomethylene-3-indanone, exemplified by ITIC[12] and IEIC.[13] Relative to traditional fullerene acceptors, A–D–A type FREAs can be readily synthesized and purified, and their optical bandgap and energy levels can be readily tuned. FREAs exhibit much stronger absorption in the visible and even near-infrared region.[14–17] FREA-based OSCs can achieve higher power conversion efficiencies (PCEs),[18–23] greater thermal stability,[24] and longer device lifetime than their fullerene-based counterparts.[25,26] So far, most of FREAs reported in literature are based on indacenodithiophene,[12,27] fluorene,[28,29] and benzo[1,2-*b*:4,5-*b*′]dithiophene units.[30,31] These units have relatively weak intermolecular interaction, leading to relatively

J. Zhu, J. Wang, S. Dai, Prof. X. Zhan
Department of Materials Science and Engineering
College of Engineering
Key Laboratory of Polymer Chemistry and Physics of Ministry of Education
Peking University
Beijing 100871, China
E-mail: xwzhan@pku.edu.cn
J. Zhu, Y. Xu, Dr. Y. Lin
Department of Chemistry
Capital Normal University
Beijing 100048, China
E-mail: linyz@iccas.ac.cn
Z. Ke, Y. Wu, Prof. W. Ma
State Key Laboratory for Mechanical Behavior of Materials
Xi'an Jiaotong University
Xi'an 710049, China
Q. Zhang, Prof. W. You
Department of Chemistry
University of North Carolina at Chapel Hill
NC 27599, USA
The ORCID identification number(s) for the author(s) of this article can be found under https://doi.org/10.1002/adma.201704713.

DOI: 10.1002/adma.201704713

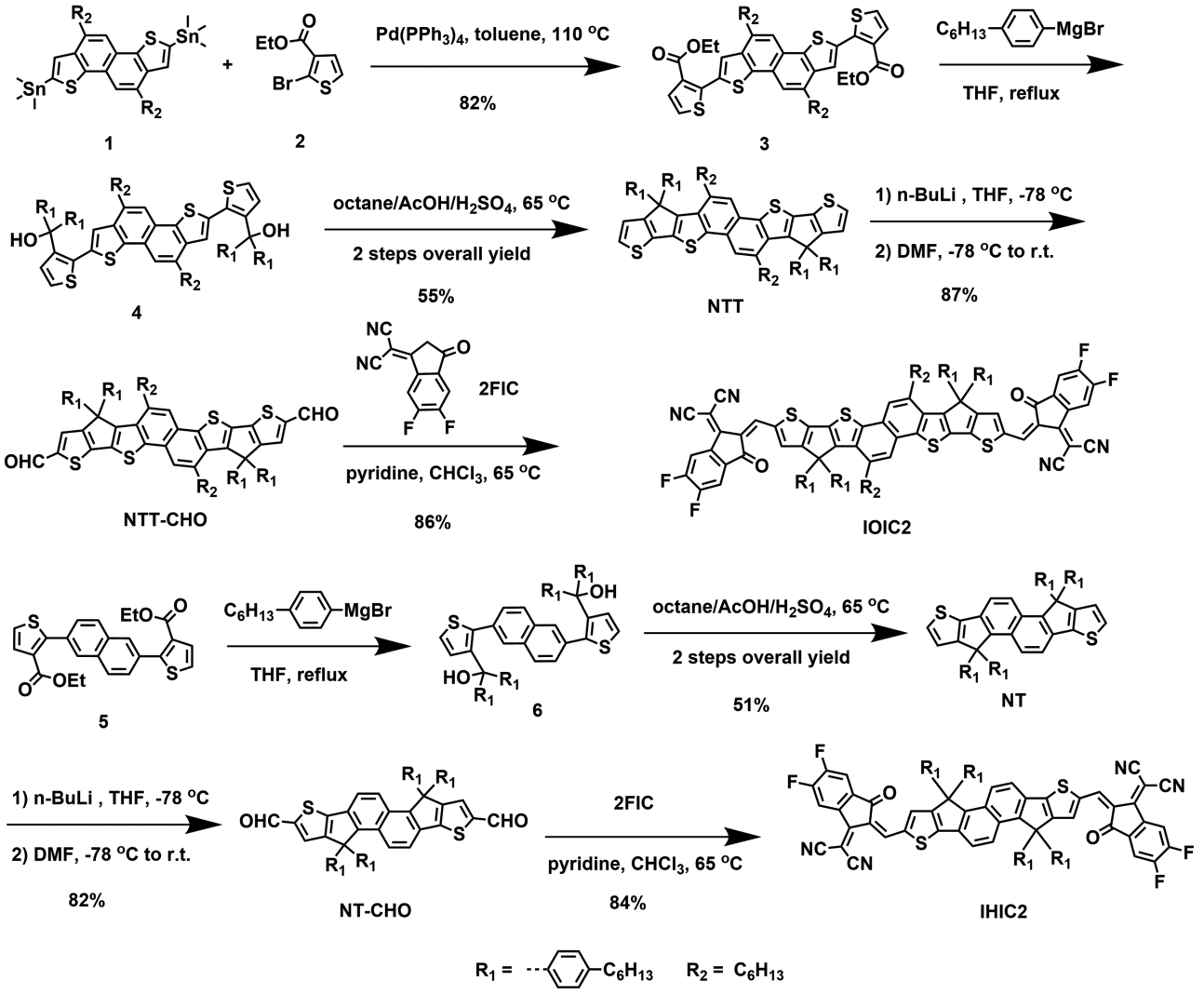

Scheme 1. Synthetic routes to IOIC2 and IHIC2.

weak molecular packing, and, therefore, low charge mobility (generally 10^{-5}–10^{-4} cm^2 V^{-1} s^{-1}), which is much lower than those of fullerene acceptors (10^{-3}–10^{-2} cm^2 V^{-1} s^{-1}).[12,29,31] The low mobility of nonfullerene acceptors is an apparent limitation for achieving high fill factor (FF) of the thicker OSCs.[11] Thus, there remains a need to develop high-mobility nonfullerene acceptors based on planar and large fused-ring cores that possess strong π stacking.

In this work, we first designed and synthesized a planar fused octacyclic core (NTT) by fusing naphtho[1,2-*b*:5,6-*b*′]dithiophene (NDT) with two cyclopentadienylthiophenes (**Scheme 1**). We chose NDT because it has a highly planar structure and strong molecular packing and has been used for constructing p-type organic semiconductors that have shown high charge carrier mobilities. For example, Takimiya and co-workers reported a series of NDT-based small molecules and polymers that exhibited promising performance in organic field-effect transistors (hole mobility as high as 0.8 cm^2 V^{-1} s^{-1}) and as donors in OSCs (PCE as high as 8.2%).[32–34] Taking this newly developed electron-rich NTT core to couple with electron-deficient 2-(5,6-difluoro-3-oxo-2,3-dihydro-1H-inden-1-ylidene)malononitrile (2FIC) unit, we next synthesized a nonfullerene acceptor 2,2′-((2Z,2′Z)-(5,10-dihexylnaphtho[1,2-*b*:5,6-*b*′]di(4,4-bis(4-hexylphenyl)-4H-cyclopenta[2,1-*b*:3,4-*b*′]dithiophene-2,7-diyl) bis(5,6-difluoro-3-(dicyanomethylene)-2-methylene-indan-1-one) (IOIC2, Scheme 1), following the A–D–A design motif. Partial fluorination of the end groups in the case of 2FIC can redshift the absorption due to enhanced intramolecular charge transfer between NDT and 2FIC and can improve electron mobility due to noncovalent F—S and F—H bonding, as we previously reported.[16] For comparison, we also synthesized a fused hexacyclic electron acceptor 2,2′-((2Z,2′Z)-(3,3,8,8-tetrakis(4-hexylphenyl)-3,8-dihydrodicyclopenta[a,f]naphtho[1,2-*b*:5,6-*b*′]-dithiophene-2,7-diyl)bis(5,6-difluoro-3-(dicyanomethylene)-2-methylene-indan-1-one) (IHIC2, Scheme 1) with naphthalene core. Relative to IHIC2 with a smaller core, IOIC2 based on a larger π-conjugation core exhibits (a) higher energy levels, (b) redshifted absorption spectra, and (c) higher electron mobility (1×10^{-3} cm^2 V^{-1} s^{-1}), which are beneficial to (a) increasing open-circuit voltage (V_{OC}), (b) short-circuit current density (J_{SC}),

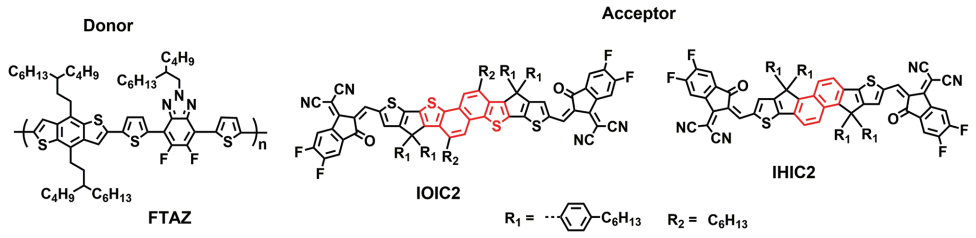

Scheme 2. Chemical structures of FTAZ, IOIC2, and IHIC2.

and (c) FF. Indeed, as-cast OSCs based on IOIC2: FTAZ[35] (**Scheme 2**) without any additional treatment yield PCEs of up to 11.2%, which is much higher than that of the control devices based on IHIC2: FTAZ (7.45%). With 0.2% 1,8-diiodooctane (DIO) as solvent additive to optimize the morphology, the PCE of IOIC2: FTAZ-based devices can be improved to 12.3%, which is among the highest efficiency values reported for single-junction binary-blend OSCs.[36]

The molecular geometries and electronic properties of IOIC2 and IHIC2 were investigated with density functional theory calculations at B3LYP/6-31G* level. Both IOIC2 and IHIC2 possess planar backbone (Figure S1, Supporting Information), which would be beneficial to intermolecular π–π interactions. The calculated highest occupied molecular orbital (HOMO) and lowest unoccupied molecular orbital (LUMO) energy levels of IOIC2 are −5.51 and −3.39 eV, respectively, higher than those of IHIC2 (HOMO: −5.68 eV; LUMO: −3.46 eV). The synthetic routes to IOIC2 and IHIC2 are illustrated in Scheme 1. $Pd(PPh_3)_4$ catalyzed Stille coupling reaction between compounds **1** and **2** afforded intermediate compound **3**. A double nucleophilic addition of (4-hexylphenyl) magnesium bromide to the ester groups in compound **3**, followed by intramolecular cyclization via acid-mediated Friedel–Crafts reaction afforded NTT. NTT was then lithiated by *n*-butyllithium in tetrahydrofuran solution at −78 °C and subsequently quenched by dry dimethylformamide to afford aldehyde NTT-CHO. A Knoevenagel condensation between NTT-CHO and 2FIC yielded the final product IOIC2. IHIC2 was synthesized via a similar approach by using compound **5** instead of compound **3**. All new compounds were characterized by high-resolution mass spectrometry, FT-IR, ^{1}H-NMR, ^{13}C-NMR, and elemental analysis (see the Supporting Information). Both IOIC2 and IHIC2 have good solubility in common organic solvents such as chloroform and *o*-dichlorobenzene at room temperature, and excellent thermal stability with decomposition temperature (T_d, 5% weight loss) at 384 and 347 °C, respectively, via thermogravimetric analysis (Figure S2a, Supporting Information). From differential scanning calorimetry, IOIC2 shows a melting point at 288 °C, while IHIC2 shows no melting peak from room temperature to 300 °C (Figure S2b, Supporting Information).

The normalized absorption spectra of IHIC2 and IOIC2 in chloroform solution (10^{-6} M) are shown in Figure S3a in the Supporting Information. IHIC2 and IOIC2 in solution exhibit strong absorption in 550–750 nm region with high molar extinction coefficients of 1.6×10^5 M^{-1} cm^{-1} at 659 nm and 1.8×10^5 M^{-1} cm^{-1} at 696 nm, respectively. In the thin film (Figure S3b, Supporting Information), IHIC2 and IOIC2 show the maximum absorption peaks at 682 and 730 nm, respectively. Relative to their solutions, the maximum absorption peaks of IHIC2 and IOIC2 films redshift by 23 and 34 nm, respectively. The larger redshift in IOIC2 suggests that IOIC2 has stronger molecular self-organization than IHIC2 in the film. The optical bandgap of IHIC2 and IOIC2 films are 1.66 and 1.55 eV, estimated from the absorption onset at 745 and 801 nm, respectively. Relative to IHIC2, the broader absorption spectrum of IOIC2 benefits the utilization of sunlight.

The HOMO and LUMO energies of IHIC2 film are estimated to be −5.69 and −3.86 eV from the onset oxidation and reduction potentials, respectively, from electrochemical cyclic voltammetry (Figure S3c, Supporting Information). IOIC2 shows higher energy levels (HOMO = −5.41 eV; LUMO = −3.78 eV) than IHIC2 (**Figure 1**b), which can be attributed to the stronger electron-donating property of NTT core of IOIC2. The higher LUMO energy level of IOIC2 will benefit high V_{OC} in OSCs.

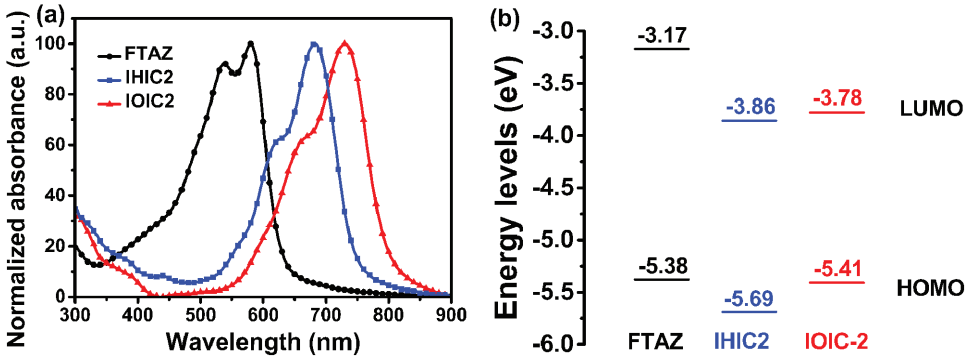

Figure 1. a) UV–vis absorption spectra of FTAZ, IHIC2, and IOIC2 in thin films. b) Energy levels of FTAZ, IHIC2, and IOIC2 estimated from cyclic voltammetry.

Table 1. Performance of the optimized OSCs based on FTAZ: acceptor (average data are obtained from 20 devices, best data in brackets).

Active layer	V_{OC} [V]	J_{SC} [mA cm^{-2}]	FF [%]	PCE [%]	Calculated J_{SC} [mA cm^{-2}]
FTAZ: IHIC2	0.774 ± 0.006	15.6 ± 0.2	60.5 ± 1.2	7.30 ± 0.18	15.1
	(0.775)	(15.7)	(61.2)	(7.45)	
FTAZ: IHIC2	0.763 ± 0.005	15.8 ± 0.3	58.4 ± 0.9	7.03 ± 0.17	15.5
0.2% DIO	(0.766)	16.1	(59.2)	(7.31)	
FTAZ: IOIC2	0.903 ± 0.003	18.4 ± 0.1	66.5 ± 0.8	11.1 ± 0.1	18.2
	(0.902)	(18.5)	(67.2)	(11.2)	
FTAZ: IOIC2	0.898 ± 0.005	19.4 ± 0.2	69.6 ± 0.5	12.1 ± 0.2	19.1
0.2% DIO	(0.900)	(19.7)	(69.3)	(12.3)	

Space charge limited current (SCLC) measurement indicates that IOIC2 has a higher electron mobility (1.0×10^{-3} cm^2 V^{-1} s^{-1}) than IHIC2 (5.0×10^{-4} cm^2 V^{-1} s^{-1}) (Figure S4, Supporting Information), which can also be ascribed to the larger NTT core. The electron mobility of IOIC2 is very close to those (10^{-3} cm^2 V^{-1} s^{-1}) of fullerene acceptors[37] and can ensure more effective charge carrier transport to the electrodes.

The wide-bandgap polymer donor FTAZ (Scheme 2) exhibits strong absorption at 400–650 nm,[35] which complements that of IHIC2 and IOIC2 (Figure 1a). The HOMO and LUMO energy levels of FTAZ also match with those of IHIC2 and IOIC2 (Figure 1b). Furthermore, FTAZ exhibits a high hole mobility (on the order of 10^{-3} cm^2 V^{-1} s^{-1}) that matches with those of IHIC2 and IOIC2.[38] Thus, to demonstrate potential application of IHIC2 and IOIC2 in OSCs as electron acceptors, we used FTAZ (M_n = 42.2 kg mol^{-1})[35] as a donor to fabricate BHJ OSCs with a structure of indium tin oxide (ITO)/ZnO/FTAZ: IHIC2 or IOIC2/MoO_3/Ag. We optimized the device fabrication conditions, such as donor/acceptor (D/A) weight ratio and DIO additive content (Tables S1 and S2, Supporting Information). **Table 1** summarizes the V_{OC}, J_{SC}, FF, and PCE of the optimized devices. The best OSC based on as-cast FTAZ: IOIC2 (1:1.5, w/w) film gives a V_{OC} of 0.902 V, J_{SC} of 18.5 mA cm^{-2}, FF of 67.2%, and PCE of 11.2%. In comparison, the best OSCs based on as-cast FTAZ: IHIC2 (1:1.5, w/w) shows a V_{OC} of 0.775 V, J_{SC} of 15.7 mA cm^{-2}, FF of 61.2%, and PCE of 7.45%. Furthermore, when 0.2% DIO was used as solvent additive, the best OSC based on FTAZ: IOIC2 (1:1.5, w/w) yields an enhanced PCE of 12.3% with a V_{OC} of 0.900 V, J_{SC} of 19.7 mA cm^{-2}, and FF of 69.3%. In comparison, the best OSCs based on FTAZ: IHIC2 (1:1.5, w/w) with 0.2% DIO shows a V_{OC} of 0.766 V, J_{SC} of 16.1 mA cm^{-2}, FF of 59.2%, and PCE of 7.31% (**Figure 2**a and Table 1).

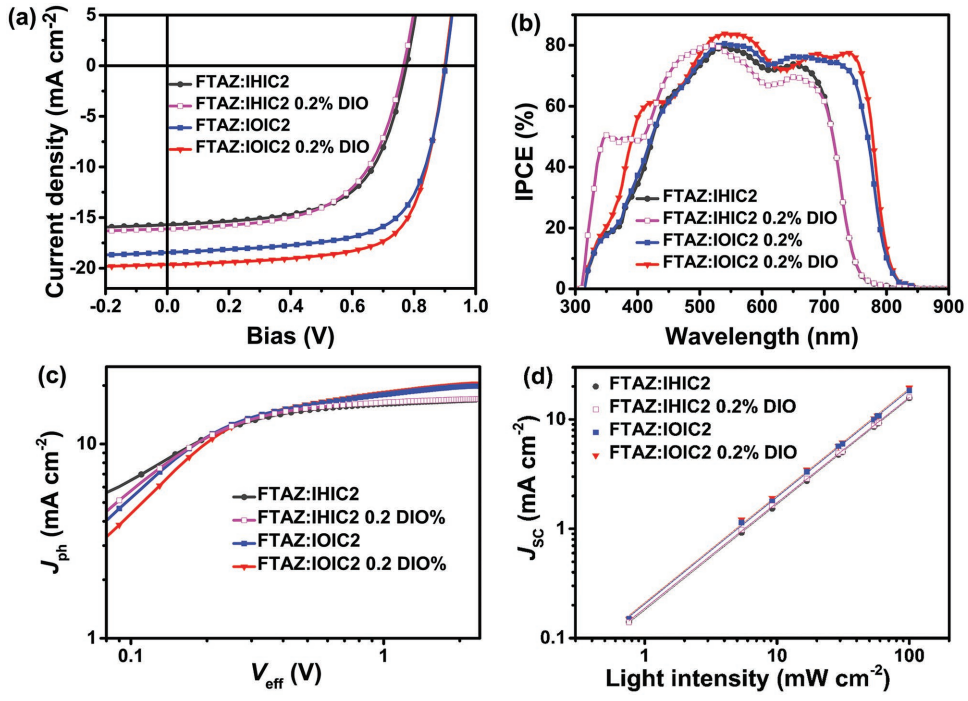

Figure 2. a) *J*–*V* curves, b) IPCE spectra, c) J_{ph} versus V_{eff} characteristics, and d) J_{SC} versus light intensity of devices with the structure ITO/ZnO/active layer/MoO_3/Ag.

Compared with the FTAZ: IHIC2 device, FTAZ: IOIC2-based devices show higher values in V_{OC}, J_{SC}, and FF. The higher V_{OC} is related to the higher LUMO level of IOIC2, while the higher J_{SC} can be attributed to redshifted absorption of IOIC2 which, together with the complementary absorption of FTAZ (Figure 1), leads to a better overlap with the solar spectrum. This enhanced absorption and J_{SC} are confirmed by the incident photon to converted current efficiency (IPCE) spectra of the optimized devices (Figure 2b). The OSCs based on FTAZ: IOIC2 show broader photoresponse extending to 820 nm; in contrast, FTAZ: IHIC2 control devices have an IPCE onset at 760 nm. The maximum IPCE value of as-cast FTAZ: IOIC2 is 80.5%, higher than that of as-cast FTAZ: IHIC2 (79.2%), indicating more efficient charge generation and collection in IOIC2-based OSCs. Furthermore, the DIO additive improves the maximum IPCE of FTAZ: IOIC2 up to 83.8%, higher than that of FTAZ: IHIC2 with 0.2% DIO (80.1%).

To probe the exciton/charge dynamics, we measured the photocurrent density (J_{ph}) versus the effective voltage (V_{eff}) to study the charge generation, dissociation, and extraction properties. In Figure 2c, at high applied voltage ($V_{eff} > 2$ V), J_{ph} reaches saturation, implying that almost all excitons are dissociated and photogenerated charge carriers are completely collected by the electrodes. The charge dissociation probability can be calculated from J_{SC}/J_{sat}.[39] The J_{SC}/J_{sat} ratio for the devices of FTAZ: IHIC2, FTAZ: IHIC2 with 0.2% DIO, FTAZ: IOIC2 and FTAZ: IOIC2 with 0.2% DIO is calculated to be 93.3%, 93.1%, 93.5%, and 94.0% under the short circuit condition, respectively, indicating that all OSCs have efficient charge dissociation and collection.

To gain insights into charge recombination in the active layers, light intensity-dependent photocurrent measurement was carried out for the optimized devices. J_{SC} under illumination of different incident light intensity (P_{light}) was measured and a power-law dependence of J_{SC} on light intensity was determined: $J_{SC} \propto P_{light}^{\alpha}$ (Figure 2d).[40] For extreme conditions, α equals to 0.75 when space charge buildup reaches fundamental limit, while α equals to 1 when no space charge exists. The α values of FTAZ: IHIC2, FTAZ: IHIC2 with 0.2% DIO, FTAZ: IOIC2, and FTAZ: IOIC2 with 0.2% DIO are 0.967, 0.965, 0.978, and 0.979, respectively, suggesting negligible bimolecular charge recombination under the short circuit condition in all these devices.

To study the initial stability of the best device, stress (such as heat and light) was employed. For thermal stability test, the devices based on FTAZ: IOIC2 with 0.2% DIO were continuously heated at 100 °C for 300 min; the PCE decreases by a factor of ≈20% and then keeps almost stable (Figure S5a, Supporting Information). The light stability of the device based on FTAZ: IOIC2 with 0.2% DIO was tested under continuous AM 1.5G illumination at 100 mW cm^{-2}; after continuous illumination for 120 min, the PCE retains 74% of its original value (Figures S5b, Supporting Information).

SCLC method is employed to measure hole and electron mobilities of FTAZ: IHIC2, FTAZ: IOIC2, and FTAZ: IOIC2 with 0.2% DIO blended films (Figure S6 and Table S3, Supporting Information). The as-cast FTAZ: IHIC2 blended film exhibits a hole mobility (μ_h) of 1.8×10^{-3} cm^2 V^{-1} s^{-1} and an electron mobility (μ_e) of 2.3×10^{-5} cm^2 V^{-1} s^{-1} with a μ_h/μ_e ratio of 78. The as-cast FTAZ: IOIC2 film exhibits higher and more balanced charge mobilities ($\mu_h = 4.0 \times 10^{-3}$ cm^2 V^{-1} s^{-1}, $\mu_e = 1.4 \times 10^{-4}$ cm^2 V^{-1} s^{-1}, $\mu_h/\mu_e = 29$). The DIO additive further enhances and balances the charge mobilities of FTAZ: IOIC2 blended film ($\mu_h = 4.8 \times 10^{-3}$ cm^2 V^{-1} s^{-1}, $\mu_e = 6.8 \times 10^{-4}$ cm^2 V^{-1} s^{-1}, $\mu_h/\mu_e = 7$). The higher and more balanced charge mobilities are responsible for the higher FF in the FTAZ: IOIC2- based devices.

The morphology of the blended films of FTAZ: IHIC2, FTAZ: IOIC2, and FTAZ: IOIC2 with 0.2% DIO was studied by transmission electron microscopy (TEM), grazing incidence wide-angle X-ray scattering (GIWAXS), and resonant soft X-ray scattering (R-SoXS). In the TEM images (Figure S7, Supporting Information), the blended films of FTAZ: IHIC2 and FTAZ: IOIC2 show low contrast, while FTAZ: IOIC2 with 0.2% DIO shows visible contrast, suggesting DIO improves the crystallinity of FTAZ: IOIC2 film. The molecular packing information was provided by GIWAXS[41] (**Figure 3**). The (100) diffraction peak ($q \approx 0.33$ Å^{-1}) of the neat IOIC2 film is stronger than the (100) diffraction peak ($q \approx 0.37$ Å^{-1}) of the IHIC2 neat film. Also, the IOIC2 shows the pronounced π–π stacking peak ($q \approx 1.71$ Å^{-1}), but IHIC2 does not, which can be ascribed to the extended fuse ring of NTT in IOIC2. The improved π–π stacking in IOIC2 benefits the charge transport, leading to higher electron mobility of IOIC2 than IHIC2. According to the location of peaks displayed in the pure films, the crystallinity of both donor and acceptor in the blend can be inferred by fitting scattering peaks with Gauss distributions. In the FTAZ: IHIC2 blend, IHIC2 displays poor crystallinity with weak (100) diffraction peak ($q \approx 0.37$ Å^{-1}), while FTAZ exhibits stronger (100) diffraction peak ($q \approx 0.33$ Å^{-1}) and π–π stacking peak ($q \approx 1.71$ Å^{-1}). In the FTAZ: IOIC2 blend, (100) diffraction peak ($q \approx 0.33$ Å^{-1}) and π–π stacking peak ($q \approx 1.71$ Å^{-1}) of FTAZ and IOIC2 are overlapped, and it is hard to split the donor and acceptor peaks even by fitting scattering peaks with Gauss distributions. In contrast, all the diffraction peaks in the FTAZ: IOIC2 blended film are sharper and stronger than those in FTAZ: IHIC2, suggesting higher crystallinity. All the diffraction peaks in the FTAZ: IOIC2 blended film become sharper when the 0.2% DIO additive was used during the processing, indicating that the DIO additive helps to form higher degree of molecular ordering in the blended film, which was also confirmed by the TEM images. The π–π stacking coherence length of FTAZ: IOIC2 without and with DIO was calculated via Scherrer equation[42] to be 1.6 and 2.9 nm, respectively. A longer π–π stacking coherence length is beneficial to the intermolecular charge transport, which can explain why FTAZ: IOIC2 blend processed with the DIO additive achieved higher charge carrier mobility.

R-SoXS[43,44] was further used to probe the phase separation in FTAZ: IHIC2 and FTAZ: IOIC2 blended films processed without and with DIO (**Figure 4**). The photon energy of 285.2 eV was selected in order to obtain the most intensified material contrast. The domain size is half of characteristic mode length (domain spacing, ξ) which can be calculated by $\xi_{mode} = 2\pi/q_{mode}$. The FTAZ: IHIC2 and FTAZ: IOIC2 films without and with DIO display similar phase separation with domain sizes of ≈18 nm, which is close to exciton diffusion length and beneficial for the exciton dissociation. Additionally, R-SoXS can also reveal the average composition variations (relative domain

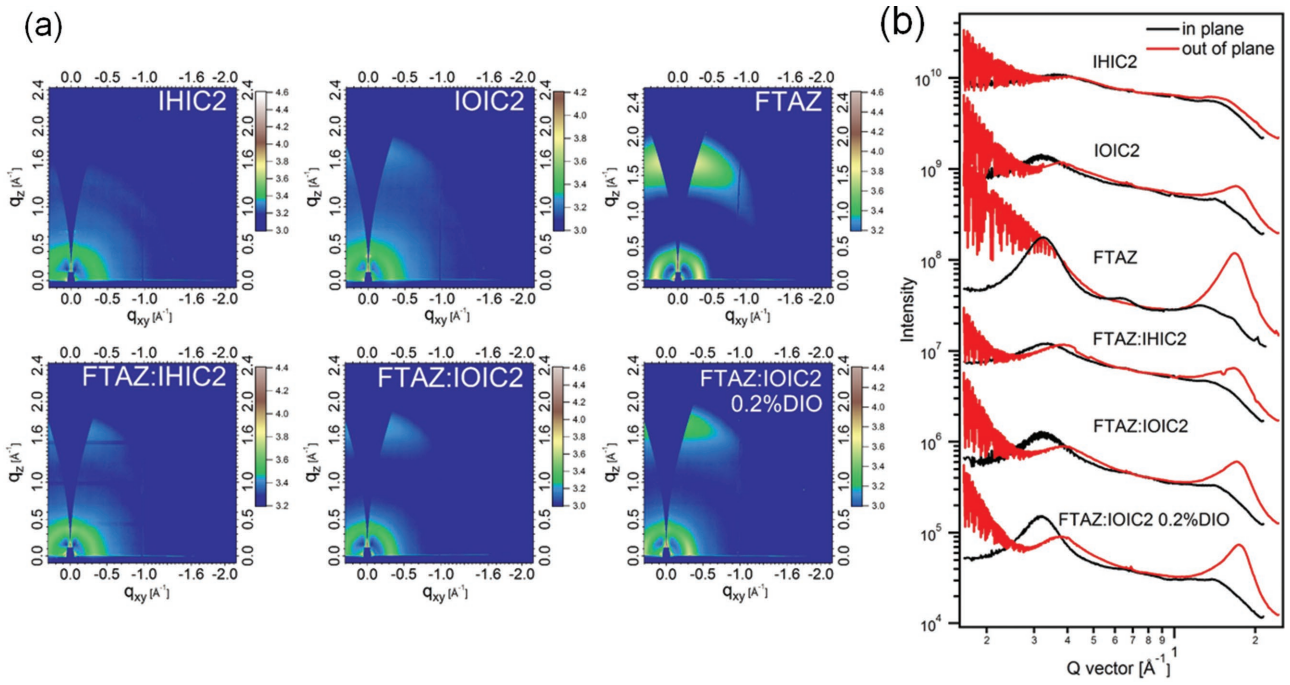

Figure 3. a) 2D GIWAXS patterns and b) scattering profiles of in-plane and out-of-plane for neat and blended films.

purity) via integrating scattering profiles (TSI = $\int_{q_1}^{q_2} I(q)q^2\,\mathrm{d}q$), TSI is total scattering intensity). The higher TSI implies the purer average domains. The relative domain purity of FTAZ: IHIC2 and FTAZ: IOIC2 without and with DIO was calculated to be 0.94, 0.91, and 1, respectively. When the domain size is relatively small, the higher domain purity would minimize the possibility of bimolecular recombination and ameliorate charge transport.

In summary, we designed and synthesized a fused octacyclic electron acceptor IOIC2 based on high-mobility naphthodithiophene core. Compared with naphthalene-based IHIC2, the NTT core in IOIC2 has a larger extended π-conjugation with a stronger electron-donating ability and stronger intermolecular π–π stacking. Thus, IOIC2 has shown higher energy levels, broader absorption spectra, and higher electron mobility values. Finally, paired with the FTAZ polymer donor that has matched energy levels and complementary absorption spectrum, the IOIC2-based OSCs show higher values in V_{OC}, J_{SC}, FF, and finally much higher PCE than the IHIC2-based OSCs. As-cast OSCs based on FTAZ: IOIC2 without any additional treatment yield PCEs of up to 11.2%, much higher than that of the control devices based on FTAZ: IHIC2 (7.45%). The performance of the FTAZ: IOIC2-based devices can be further improved with 0.2% DIO, and the champion device exhibits a PCE of 12.3% with V_{OC} of 0.900 V, J_{SC} of 19.7 mA cm^{-2}, and FF of 69.3%. The 12.3% PCE is among the highest values reported for single-junction binary-blend-based OSCs. These results demonstrate the great potential of naphthodithiophene for constructing high-performance nonfullerene acceptors. Indeed, extending π-conjugation of electron-donating fused-ring units in FREAs appears to be a promising approach to raise energy levels, enhance absorption and electron mobility, and finally achieve high efficiencies in nonfullerene-based OSCs.

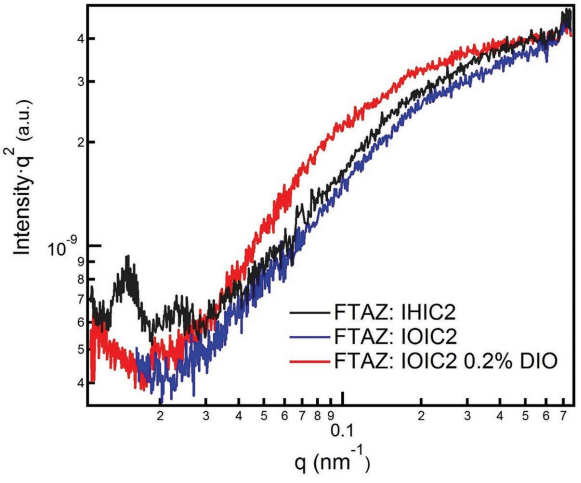

Figure 4. R-SoXS profiles in log scale for FTAZ: IHIC2, FTAZ: IOIC2, and FTAZ: IOIC2 with 0.2% DIO additive.

Supporting Information

Supporting Information is available from the Wiley Online Library or from the author.

Acknowledgements

X.Z. wishes to thank the National Natural Science Foundation of China (NSFC) (Nos. 91433114 and 21734001). Y.L. thanks the NSFC (21504058). Q.Z. and W.Y. thank the National Science Foundation (NSF) (DMR-1507249 and CBET-1639429). W.M. thanks the Ministry of Science

and Technology of China (2016YFA0200700) and NSFC (21504066 and 21534003). X-ray data were acquired at beamlines 7.3.3 and 11.0.1.2 at the Advanced Light Source, which was supported by the Director, Office of Science, Office of Basic Energy Sciences, of the U.S. Department of Energy under Contract No. DE-AC02-05CH11231. The authors thank Chenhui Zhu at beamline 7.3.3 and Cheng Wang at beamline 11.0.1.2 for assistance with data acquisition.

Conflict of Interest

The authors declare no conflict of interest.

Keywords

fused-ring electron acceptors, naphthodithiophene, nonfullerene acceptors, organic solar cells

Received: August 18, 2017
Revised: October 3, 2017
Published online: November 23, 2017

[1] A. J. Heeger, *Adv. Mater.* **2014**, *26*, 10.
[2] S. Gunes, H. Neugebauer, N. S. Sariciftci, *Chem. Rev.* **2007**, *107*, 1324.
[3] Y.-J. Cheng, S.-H. Yang, C.-S. Hsu, *Chem. Rev.* **2009**, *109*, 5868.
[4] F. C. Krebs, N. Espinosa, M. Hösel, R. R. Søndergaard, M. Jørgensen, *Adv. Mater.* **2014**, *26*, 29.
[5] L. Lu, T. Zheng, Q. Wu, A. M. Schneider, D. Zhao, L. Yu, *Chem. Rev.* **2015**, *115*, 12666.
[6] G. Li, R. Zhu, Y. Yang, *Nat. Photonics* **2012**, *6*, 153.
[7] G. Yu, J. Gao, J. C. Hummelen, F. Wudl, A. J. Heeger, *Science* **1995**, *270*, 1789.
[8] M. Li, K. Gao, X. Wan, Q. Zhang, B. Kan, R. Xia, F. Liu, X. Yang, H. Feng, W. Ni, Y. Wang, J. Peng, H. Zhang, Z. Liang, H.-L. Yip, X. Peng, Y. Cao, Y. Chen, *Nat. Photonics* **2017**, *11*, 85.
[9] J. Zhao, Y. Li, G. Yang, K. Jiang, H. Lin, H. Ade, W. Ma, H. Yan, *Nat. Energy* **2016**, *1*, 15027.
[10] Y. Lin, X. Zhan, *Mater. Horiz.* **2014**, *1*, 470.
[11] Y. Lin, X. Zhan, *Adv. Energy Mater.* **2015**, *5*, 1501063.
[12] Y. Lin, J. Wang, Z. G. Zhang, H. Bai, Y. Li, D. Zhu, X. Zhan, *Adv. Mater.* **2015**, *27*, 1170.
[13] Y. Lin, Z.-G. Zhang, H. Bai, J. Wang, Y. Yao, Y. Li, D. Zhu, X. Zhan, *Energy Environ. Sci.* **2015**, *8*, 610.
[14] F. Liu, Z. Zhou, C. Zhang, J. Zhang, Q. Hu, T. Vergote, F. Liu, T. P. Russell, X. Zhu, *Adv. Mater.* **2017**, *29*, 1606574.
[15] W. Wang, C. Yan, T. K. Lau, J. Wang, K. Liu, Y. Fan, X. Lu, X. Zhan, *Adv. Mater.* **2017**, *29*, 1701308.
[16] S. Dai, F. Zhao, Q. Zhang, T. K. Lau, T. Li, K. Liu, Q. Ling, C. Wang, X. Lu, W. You, X. Zhan, *J. Am. Chem. Soc.* **2017**, *139*, 1336.
[17] Y. Lin, Q. He, F. Zhao, L. Huo, J. Mai, X. Lu, C.-J. Su, T. Li, J. Wang, J. Zhu, Y. Sun, C. Wang, X. Zhan, *J. Am. Chem. Soc.* **2016**, *138*, 2973.
[18] Y. Cui, H. Yao, B. Gao, Y. Qin, S. Zhang, B. Yang, C. He, B. Xu, J. Hou, *J. Am. Chem. Soc.* **2017**, *139*, 7302.
[19] S. Chen, Y. Liu, L. Zhang, P. C. Y. Chow, Z. Wang, G. Zhang, W. Ma, H. Yan, *J. Am. Chem. Soc.* **2017**, *139*, 6298.
[20] F. Liu, Z. Zhou, C. Zhang, T. Vergote, H. Fan, F. Liu, X. Zhu, *J. Am. Chem. Soc.* **2016**, *138*, 15523.
[21] Y. Yang, Z. G. Zhang, H. Bin, S. Chen, L. Gao, L. Xue, C. Yang, Y. Li, *J. Am. Chem. Soc.* **2016**, *138*, 15011.
[22] Y. Lin, F. Zhao, Y. Wu, K. Chen, Y. Xia, G. Li, S. K. Prasad, J. Zhu, L. Huo, H. Bin, Z. G. Zhang, X. Guo, M. Zhang, Y. Sun, F. Gao, Z. Wei, W. Ma, C. Wang, J. Hodgkiss, Z. Bo, O. Inganas, Y. Li, X. Zhan, *Adv. Mater.* **2017**, *29*, 1604155.
[23] H. Bin, L. Gao, Z. G. Zhang, Y. Yang, Y. Zhang, C. Zhang, S. Chen, L. Xue, C. Yang, M. Xiao, Y. Li, *Nat. Commun.* **2016**, *7*, 13651.
[24] F. Zhao, S. Dai, Y. Wu, Q. Zhang, J. Wang, L. Jiang, Q. Ling, Z. Wei, W. Ma, W. You, C. Wang, X. Zhan, *Adv. Mater.* **2017**, *29*, 1700144.
[25] D. Baran, R. S. Ashraf, D. A. Hanifi, M. Abdelsamie, N. Gasparini, J. A. Rohr, S. Holliday, A. Wadsworth, S. Lockett, M. Neophytou, C. J. Emmott, J. Nelson, C. J. Brabec, A. Amassian, A. Salleo, T. Kirchartz, J. R. Durrant, I. McCulloch, *Nat. Mater.* **2017**, *16*, 363.
[26] S. Holliday, R. S. Ashraf, A. Wadsworth, D. Baran, S. A. Yousaf, C. B. Nielsen, C. Tan, S. D. Dimitrov, Z. Shang, N. Gasparini, M. Alamoudi, F. Laquai, C. J. Brabec, A. Salleo, J. R. Durrant, I. McCulloch, *Nat. Commun.* **2016**, *7*, 11585.
[27] Y. Lin, T. Li, F. Zhao, L. Han, Z. Wang, Y. Wu, Q. He, J. Wang, L. Huo, Y. Sun, C. Wang, W. Ma, X. Zhan, *Adv. Energy Mater.* **2016**, *6*, 1600854.
[28] G. Zhang, G. Yang, H. Yan, J. H. Kim, H. Ade, W. Wu, X. Xu, Y. Duan, Q. Peng, *Adv. Mater.* **2017**, *29*, 1606054.
[29] N. Qiu, H. Zhang, X. Wan, C. Li, X. Ke, H. Feng, B. Kan, H. Zhang, Q. Zhang, Y. Lu, Y. Chen, *Adv. Mater.* **2016**, *29*, 1604964.
[30] J. Wang, W. Wang, X. Wang, Y. Wu, Q. Zhang, C. Yan, W. Ma, W. You, X. Zhan, *Adv. Mater.* **2017**, *29*, 1702125.
[31] B. Kan, H. Feng, X. Wan, F. Liu, X. Ke, Y. Wang, Y. Wang, H. Zhang, C. Li, J. Hou, Y. Chen, *J. Am. Chem. Soc.* **2017**, *139*, 4929.
[32] S. Shinamura, I. Osaka, E. Miyazaki, A. Nakao, M. Yamagishi, J. Takeya, K. Takimiya, *J. Am. Chem. Soc.* **2011**, *133*, 5024.
[33] I. Osaka, T. Abe, S. Shinamura, K. Takimiya, *J. Am. Chem. Soc.* **2011**, *133*, 6852.
[34] I. Osaka, T. Kakara, N. Takemura, T. Koganezawa, K. Takimiya, *J. Am. Chem. Soc.* **2013**, *135*, 8834.
[35] S. C. Price, A. C. Stuart, L. Yang, H. Zhou, W. You, *J. Am. Chem. Soc.* **2011**, *133*, 4625.
[36] W. Zhao, S. Li, H. Yao, S. Zhang, Y. Zhang, B. Yang, J. Hou, *J. Am. Chem. Soc.* **2017**, *139*, 7148.
[37] L. Dou, J. You, Z. Hong, Z. Xu, G. Li, R. A. Street, Y. Yang, *Adv. Mater.* **2013**, *25*, 6642.
[38] W. Li, S. Albrecht, L. Yang, S. Roland, J. R. Tumbleston, T. McAfee, L. Yan, M. A. Kelly, H. Ade, D. Neher, W. You, *J. Am. Chem. Soc.* **2014**, *136*, 15566.
[39] V. D. Mihailetchi, L. J. Koster, J. C. Hummelen, P. W. Blom, *Phys. Rev. Lett.* **2004**, *93*, 216601.
[40] I. Riedel, J. Parisi, V. Dyakonov, L. Lutsen, D. Vanderzande, J. C. Hummelen, *Adv. Funct. Mater.* **2004**, *14*, 38.
[41] A. Hexemer, W. Bras, J. Glossinger, E. Schaible, E. Gann, R. Kirian, A. MacDowell, M. Church, B. Rude, H. Padmore, *J. Phys.: Conf. Ser.* **2010**, *247*, 012007.
[42] D.-M. Smilgies, *J. Appl. Cryst.* **2013**, *46*, 286.
[43] E. Gann, A. T. Young, B. A. Collins, H. Yan, J. Nasiatka, H. A. Padmore, H. Ade, A. Hexemer, C. Wang, *Rev. Sci. Instrum.* **2012**, *83*, 045110.
[44] Y. Wu, Z. Wang, X. Meng, W. Ma, *Prog. Chem.* **2017**, *29*, 93.